Two-dimensional bicontinuous structures from symmetric surface-directed spinodal decomposition in thin films

Michael B. Wise and Paul C. Millett*
Department of Mechanical Engineering, University of Arkansas, Fayetteville, Arkansas 72701, USA

(Received 9 April 2018; revised manuscript received 12 June 2018; published 6 August 2018)

We present numerical simulations of symmetric surface-directed spinodal decomposition in thin films with varying film thickness and film composition. The simulations utilize a Cahn-Hilliard model to describe phase separation kinetics in confined film geometries. The systems consist of two phases: a wetting phase that completely wets the top and bottom surfaces, and a nonwetting phase. Three distinct morphologies emerge including a discrete nonwetting morphology, a discrete wetting morphology, as well as a unique two-dimensional bicontinuous morphology that forms for specific values of film thickness and composition. The morphologies are analyzed with a Hoshen-Kopelman algorithm to quantify the degree of continuity of the nonwetting phase, and a morphology map is presented to guide future work.

DOI: 10.1103/PhysRevE.98.022601

I. INTRODUCTION

The physical characteristics associated with phase separation in immiscible mixtures have been widely studied for many decades [1–5]. Topics of particular interest include the morphological structure that develops in the early and late stages of separation, the rate of domain growth versus time, and the influence of geometrical confinement on the separation process. The multiphase morphologies that develop in immiscible systems explicitly govern macroscopic properties such as viscosity (in the case of fluidic systems such as emulsions) and strength (in the case of solid systems such as alloys or polymer blends). From a materials processing standpoint, a multiphase morphology can serve as a template to fabricate porous materials or membranes for many technological applications [6–9].

Bulk phase separation driven by thermodynamic demixing forces is well understood in both diffusion-governed and hydrodynamic-governed systems [2,5,10]. Following the nucleation stage, microscopic phase domains, formed either by spinodal decomposition or discrete nucleation events, enter into power-law scaling regimes associated with the growth of their average domain size. The morphology coarsens in a self-similar manner indefinitely in time, or until the characteristic domain size becomes comparable with the macroscopic material dimensions.

The phase separation process is altered by the presence of a surface, which will generally have unequal interactions with the two components in the system. Surface-directed spinodal decomposition (SDSD) has been shown to occur at air and/or substrate interfaces where one component preferentially wets the interface [11–17], thereby leading to the enrichment of one phase along that interface [12,13]. Initial works by Guenoun and coworkers found that the formation of a wetting layer and its corresponding depletion region caused an increased growth rate for adjacent domains of the nonwetting component [11]. Several experiments [17–19] and models [20–26] were designed for the purpose of studying this interplay and its implications on late-stage morphology. Reviews of SDSD summarize these efforts [27,28]. Many experimental works focus on asymmetric SDSD, typically consisting of a multiphase film in contact with a substrate below and an air interface above, whereby the two interfaces generally exhibit different wetting characteristics.

On the other hand, symmetric SDSD refers to the spinodal decomposition that occurs within a film constrained between two identical parallel substrates with equal wetting characteristics. Numerical simulations by Das and coworkers [29,30], Puri [31], and Hore and Laradji [32] of symmetric SDSD found that early-stage spinodal decomposition with bicontinuous domains evolved into a morphology consisting of two wetting layers connected by a random array of discrete columnar structures (of the wetting phase) that spanned the internal nonwetting phase. This structure was observed earlier by Composto's group in experiments involving binary polymer films [18]. The through-thickness columns coarsen in time and, in later stages, reduce the thickness of the wetting layers (but not to the point where the wetting layers break). These studies, however, focused on a specific range of thicknesses and blend compositions, which left the parameter space largely unexplored.

It has been demonstrated that phase domain growth laws are altered below a certain film thickness, which some have reported to be 1.5 times the spinodal wavelength [16,17]. One of the most comprehensive thickness-variation studies was performed by Chung and Composto [33], during which they discovered the potential for stable, nearly bicontinuous morphologies. While structures seen in this experiment did tend to break down into discrete domains, their results imply that one could use the thickness of a confined film to tune thin-film morphology. In addition, while previous experiments studied a single composition, it would be logical to assume that similar effects could be achieved by altering the film

*pmillett@uark.edu

FIG. 1. Diagram showing the thin film morphology with layers of the wetting phase adjacent to the top and bottom substrates, and internal domains of the nonwetting phase.

composition. Indeed, recent work by our group has shown that unique two-dimensional bicontinuous structures can form with asymmetric compositions in very thin films [34]. The phase separation process in this study [34] was halted by nanoparticle jamming at the phase interfaces, so it was not clear if late-stage coarsening would involve a transition from a bicontinuous morphology to a discrete one.

This paper describes a numerical simulation study of the effects of symmetric, preferential wetting on phase separation in thin-film confinement, with a particular focus on the influence of composition and film thickness. A Cahn-Hilliard-Cook (CHC) model with modified free energy was utilized to simulate symmetric SDSD with complete surface wetting for long evolutions well into the late-stage coarsening regime. We employed a cluster enumeration algorithm to determine the degree of bicontinuity within the film throughout time, which allowed us to quantitatively classify morphology type as either bicontinuous or discrete. A morphology map was constructed to relate morphology with composition and film thickness for symmetric SDSD. The confined phase separation we observe has potential applications in membrane science.

II. METHODS

Following the approach of Puri, Binder, and others [21–23], our numerical simulations utilize a CHC equation to model the confined phase separation process within a constrained thin film consisting of a wetting phase with volume fraction ϕ_W and a nonwetting phase with volume fraction $\phi_{\rm NW}$ (see schematic in Fig. 1). Due to volume conservation, the binary system can be described with a single order parameter $\phi = \phi_{\rm NW} - \phi_W$. The kinetic equation is written as

$$\frac{\partial \phi}{\partial t} = \nabla \cdot (M \nabla \mu) + \zeta, \tag{1}$$

where M is a mobility parameter and μ is a chemical potential defined as the variational derivative of a free energy functional F, with respect to ϕ, $\mu = \delta F/\delta\phi$. ζ is a small (volume conserving) random fluctuation term that models thermal noise in the field. The free energy functional is

$$F = \int [f(\phi) + \kappa(\nabla\phi)^2] dV, \tag{2}$$

where $f(\phi)$ is the bulk free energy density and the gradient term accounts for the phase interfacial energy. The functional

FIG. 2. Schematic of the $B(z)$ function described in Eq. (6) used to induce preferential wetting on the top and bottom z boundaries.

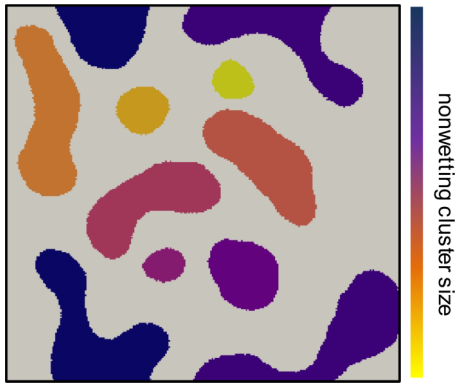

FIG. 3. The Hoshen-Kopelman algorithm identifies individual domains of the nonwetting phase and tabulates the volume of each domain. This image shows the cross section through the midplane of the film, where the colored regions are nonwetting phase domains colored according to their size.

form of the bulk free energy density is expressed as

$$f = w(f_{pp} + f_{ps}), \tag{3}$$

where f_{pp} accounts for interactions between the wetting phase and the nonwetting phase, f_{ps} for phase-surface interactions, and w is a scaling coefficient. These terms are defined by

$$f_{pp} = \phi^4/4 - \phi^2/2, \tag{4}$$

$$f_{ps} = B(z)(\phi^2 + 2\phi)/2. \tag{5}$$

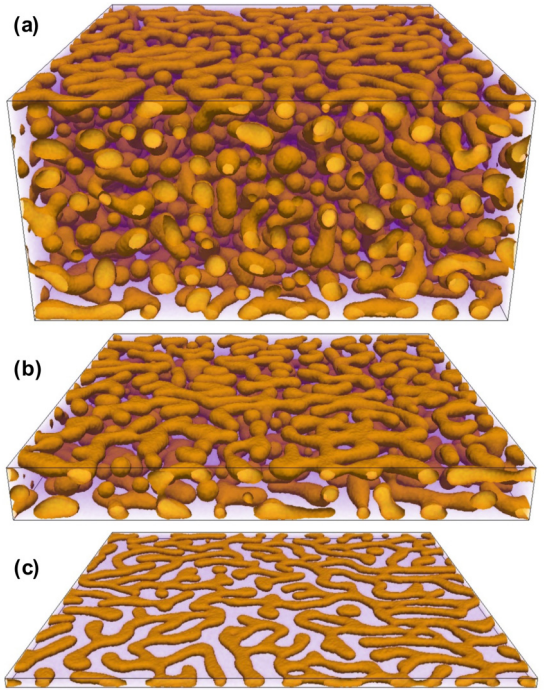

FIG. 4. Thin film morphologies with symmetric SDSD and varying thickness at a simulation time of $\tau = 7500$. The volume fraction of the nonwetting phase is $\bar{\phi}_{\rm NW} = 0.256$. The film thicknesses are (a) $n_z = 256\,\delta$, (b) $n_z = 64\,\delta$, and (c) $n_z = 16\,\delta$. Note that the wetting phase has been rendered a very transparent shade to visualize the internal nonwetting phase (orange).

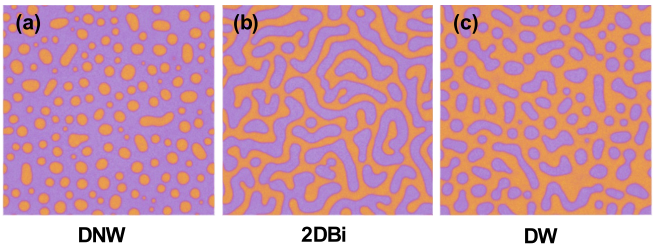

FIG. 5. Top-down views of the film morphology (at the midplane cross section) for varying compositions: (a) $\bar{\phi}_{\mathrm{NW}} = 0.200$ resulting in a discrete-non-wetting (DNW) morphology, (b) $\bar{\phi}_{\mathrm{NW}} = 0.275$ resulting in a 2D-bicontinuous (2DBi) morphology, and (c) $\bar{\phi}_{\mathrm{NW}} = 0.325$ resulting in a discrete-wetting (DW) morphology. The simulation time is $\tau = 2500$ and the film thickness is $n_z = 20\,\delta$. The nonwetting phase is colored orange, and the wetting phase colored purple.

Here, f_{pp} is a commonly used polynomial double-well function with minima at $\phi = \pm 1$ associated with the wetting ($\phi = -1$) and nonwetting ($\phi = 1$) phases. The f_{ps} term distorts the double-well curve into a single-well curve with a minimum at $\phi = -1$ (i.e., the wetting phase). $B(z)$ is a depth-dependent function that alters the energy near the confining surfaces, defined as

$$B(z) = \begin{cases} \dfrac{(4-z)\delta}{4}, & 0 < z < 4\delta \\ 0, & 4\delta < z < (n_z - 5)\delta \\ \dfrac{[z-(n_z-5)]\delta}{4} & (n_z - 5)\delta < z < n_z\delta \end{cases}, \qquad (6)$$

where δ is the simulation grid spacing, z is the height in the direction perpendicular to the confining surfaces, and n_z is the total distance between the confining surfaces. This term models the strong wetting tendency very near the surfaces, which decreases linearly to 0 within a small distance from the surfaces (see Fig. 2).

Equation (1) was solved using a psuedospectral method [35] in three-dimensional domains of size $n_x \times n_y \times n_z$. The lateral x and y dimensions were set equal with $n_x = n_y = 512\,\delta$. A variety of values of $n_z = 14$, 16, 18, 20, 22, 24, and 26 δ were chosen to understand the effects of film thickness. Composition is conserved by applying periodic boundary conditions in all directions, and the wetting condition of Eq. (6) essentially eliminates flux across the z boundaries (although a zero-flux condition, which is burdensome with the psuedospectral method, is not strictly enforced). We ensure that complete wetting layers always form along the top and bottom z boundaries. The simulations used nondimensionalized time (τ with a time step size of 0.5 τ) and length ($\delta = 1$) scales. To simplify the model as much as possible, the CHC parameters were assigned values of $M = \kappa = w = \zeta = 1$. In order to understand the effect of film composition, we systematically varied the volume-averaged fraction of the nonwetting phase with values of $\bar{\phi}_{\mathrm{NW}} = 0.25$, 0.2625, 0.275, 0.2875, and 0.3. We choose this seemingly narrow range (i.e., $0.25 < \bar{\phi}_{\mathrm{NW}} < 0.3$) based on preliminary simulations which showed that the resulting morphologies above or below this range were predictably bicontinuous or discrete for the range of film thicknesses we choose.

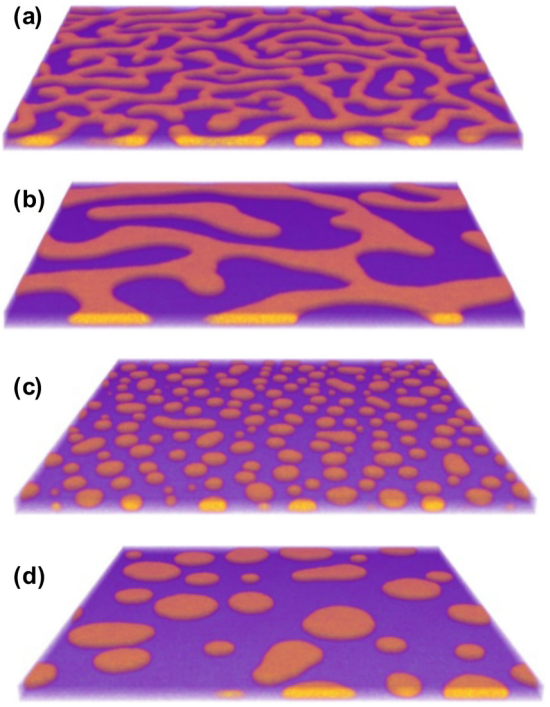

FIG. 6. Time evolution of the phase separation for compositions: (a) and (b) $\bar{\phi}_{\mathrm{NW}} = 0.275$, and (c) and (d) $\bar{\phi}_{\mathrm{NW}} = 0.200$. The early simulation snapshots in (a) and (c) are at $\tau = 2500$, and the later snapshots in (b) and (d) are at $\tau = 50\,000$.

Analysis of the simulation results was performed using the Hoshen-Kopelman algorithm [36]. This algorithm efficiently identifies and labels individual phase domains represented by an order parameter (in our case, ϕ) stored on a grid. Details of the algorithm can be found in the literature [36]. For the purposes of this paper, and as shown in Fig. 3, the algorithm labels all individual domains of the nonwetting phase (defined by values of $\phi > 0.2$), and stores the total volume of each domain based on the number of grid points associated with it. We then quantify the continuity of the nonwetting phase by calculating a continuity order parameter Γ_C [37]:

$$\Gamma_C = \frac{V_L}{V_T}, \qquad (7)$$

where V_L is the volume of the largest nonwetting phase domain and V_T is the total volume of the nonwetting phase. A system that is very continuous will have a Γ_C value near one, and a system with little continuity will have a Γ_C value near zero. In our analysis, a thin-film morphology is considered bicontinuous if the nonwetting phase has a value of a $\Gamma_C > 0.8$. The continuity order parameters were calculated throughout time and, in order to account for statistical variations, the reported values are averaged from 20 different independent simulations (with random initial conditions). Each simulation begins with a homogeneous distribution of the two components with some random variations in space, and the beginning of the simulation corresponds to an instantaneous quench into the unstable regime of the phase diagram, hence phase separation commences at the beginning of the simulation.

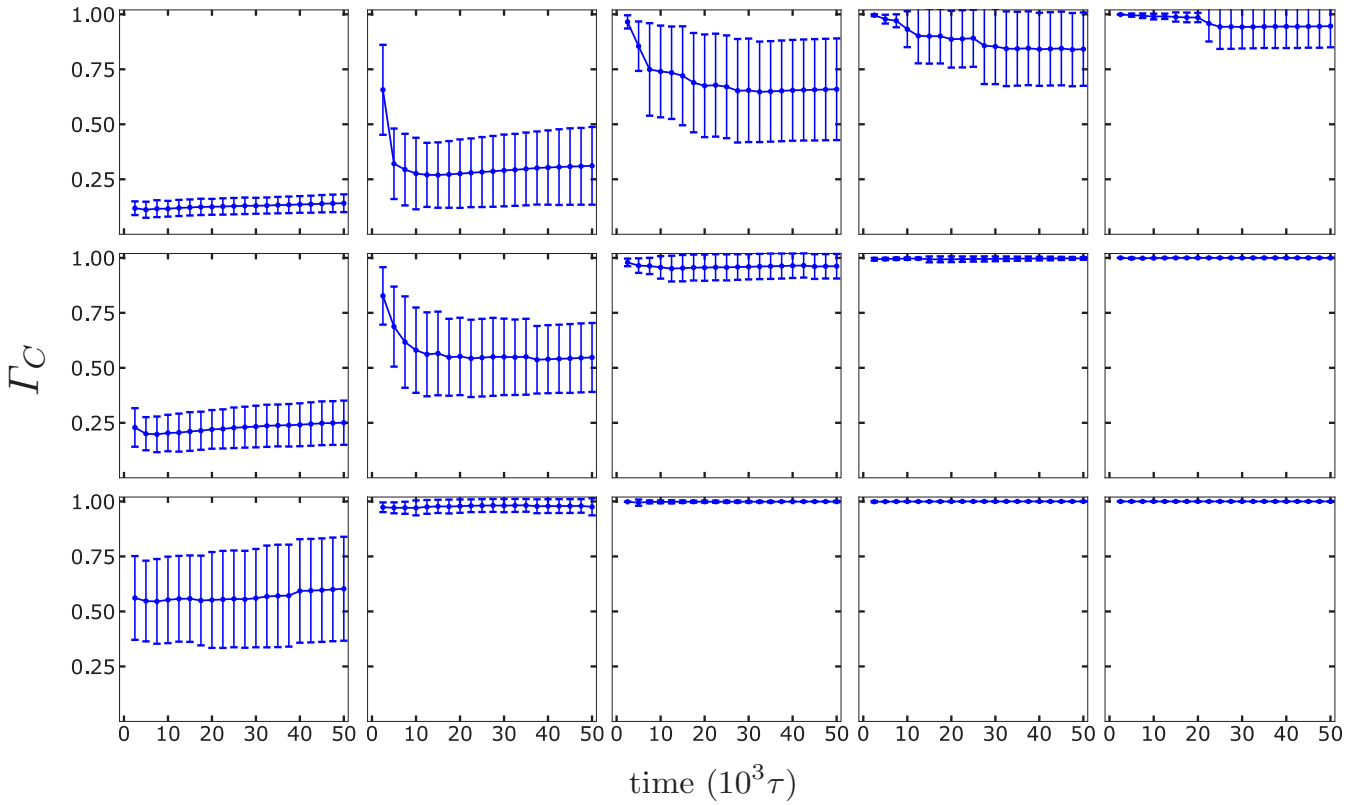

FIG. 7. Continuity factor versus time for an array of compositions and film thicknesses. The film thicknesses vary from (top row) $n_z = 26\,\delta$, (middle row) $n_z = 20\,\delta$, and (bottom row) $n_z = 14\,\delta$. The film compositions vary from the left column to the right column with values of $\bar{\phi}_{\rm NW} = 0.25$, 0.2625, 0.275, 0.2875, and 0.3. The values of Γ_C are averages of 20 independent simulations, and the error bars indicate one standard deviation.

III. RESULTS

We aim to understand the influence of film composition and film thickness on morphology with symmetric SDSD conditions. In bulk conditions, bicontinuity of the phase domains is typically limited to a narrow composition window near the critical composition (typically ∼0.5 in low molecular weight liquids; in polymer solutions, this value usually shifts to lower values in the range of 0.1–0.3). In our simple model, the critical composition is 0.5, and off-critical compositions that are below the binodal line of the phase diagram will generally undergo phase separation via nucleation of discrete domains of the minority phase that grow and coarsen with time. In a film with symmetric SDSD, this basic morphology should emerge if the distance between the wetting surfaces is adequately large.

In Fig. 4, the morphologies of thin films with symmetric SDSD are displayed with a composition of the nonwetting phase of $\bar{\phi}_{\rm NW} = 0.256$, which is certainly off-critical. For each image, the simulations have evolved to a simulation time of $\tau = 7500$ (note that the wetting phase is rendered very transparent for clarity). In Fig. 4(a), the film thickness is $n_z = 256\,\delta$, which is relatively large, and the local effects of the two wetting surfaces are not overlapping. For this thickness, the internal morphology of the nonwetting phase consists of discrete domains (as expected). However, as the film thickness is decreased, and the wetting surfaces brought closer, the morphology of the nonwetting phase transitions (rather abruptly) to a percolated state. For the smallest film thickness of $n_z = 16\,\delta$ [Fig. 4(c)], the nonwetting phase is continuous, and the system as a whole is bicontinuous, due to the fact that the wetting phase forms continuous layers on the top and bottom of the film as well as significant portions of the midsections of the film.

We identify the morphology in Fig. 4(c) as a "two-dimensional (2D) bicontinuous" morphology. The domains of the nonwetting phase resemble a percolated network of cylindrical (or, slightly flattened cylindrical) tubes. The emergence of a bicontinuous morphology with a composition so far away from the critical composition is somewhat unexpected, but is enabled by the symmetric wetting conditions of the very nearby surfaces. For these small film thicknesses, the morphology transitions in a narrow window of composition, as shown in Fig. 5. When changing the composition from $\bar{\phi}_{\rm NW} = 0.2$ to $\bar{\phi}_{\rm NW} = 0.325$, the morphology transitions from discrete domains of the nonwetting phase in the middle of the film [Fig. 5(a), labeled "DNW"], to a 2D bicontinuous morphology [Fig. 5(b), which is similar to Fig. 4(c), labeled as "2DBi"], to a morphology with discrete columns of the wetting phase spanning the internal section of the film [Fig. 5(c), which is similar to earlier experimental and theoretical observations [18,32], we label as "DW"]. It should be noted that, technically, the structure in Fig. 5(c) is also bicontinuous, as both the nonwetting and wetting phases have percolating domains, however, the wetting phase is only continuous due to the top and bottom wetting layers in the film.

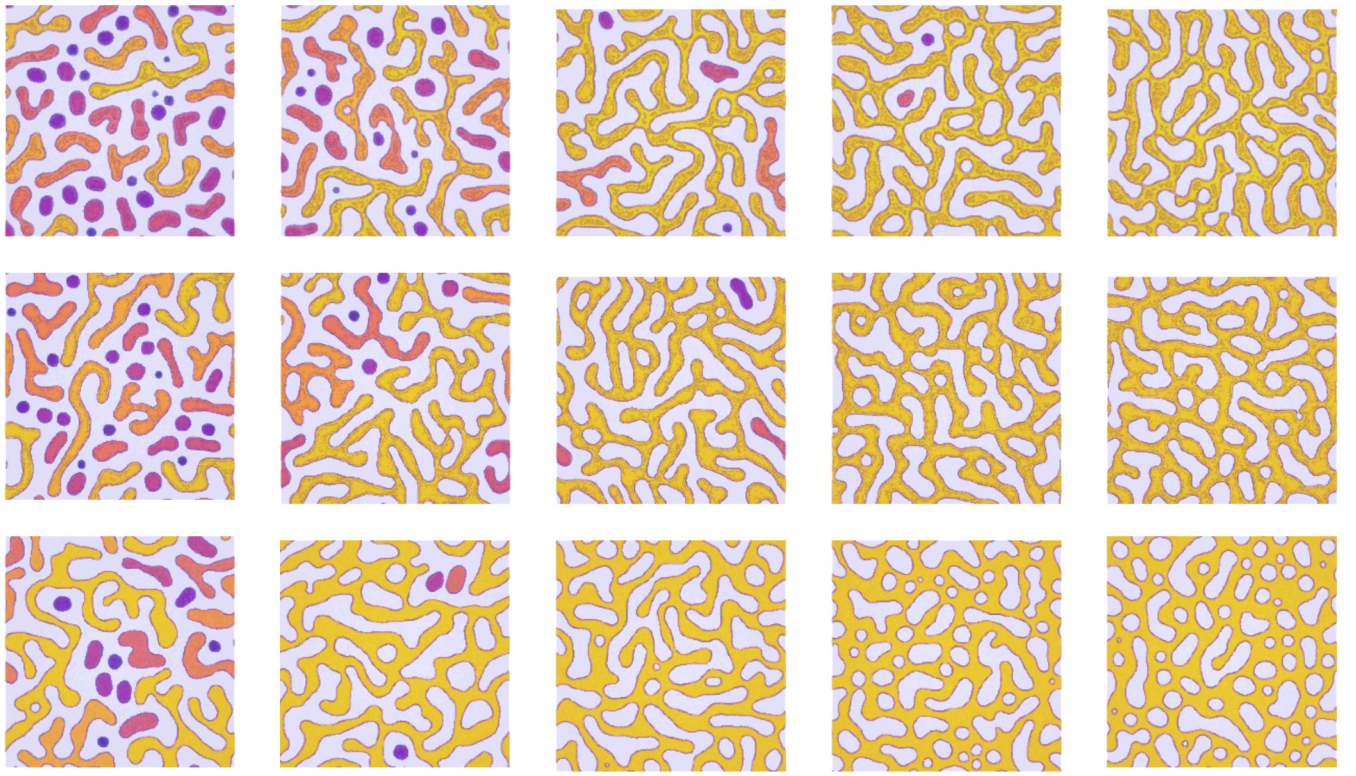

FIG. 8. Snapshots of the nonwetting phase morphology for the same array of conditions as described in Fig. 7. The nonwetting domains are colored according to their size, with yellow being the largest size (the wetting phase is colored light gray). Individual domains are identified with the Hoshen-Kopelman algorithm. Each snapshot is taken at a simulation time of $\tau = 5000$.

We now focus on the time evolution of these unique thin film morphologies. Earlier works on SDSD with critical compositions (i.e., equal quantities of the two phases) revealed that structures similar to Fig. 5(c), with two wetting layers and discrete columns of the wetting phase spanning the top and bottoms layers, evolved from a bicontinuous morphology at early stages to the discrete morphology at late stages. Therefore, we wish to explore whether the 2D bicontinuous structures of Figs. 4(c) and 5(b) remain 2D bicontinuous during late-stage coarsening. The results presented above were taken from rather early simulation times.

Figure 6 shows examples of how two distinct morphologies coarsen through time. In Figs. 6(a) and 6(b), the composition is $\bar{\phi}_{\mathrm{NW}} = 0.275$ corresponding to the 2D bicontinuous morphology, and in Figs. 6(c) and 6(d) the composition is $\bar{\phi}_{\mathrm{NW}} = 0.200$ corresponding to the discrete nonwetting morphology. Both early ($\tau = 2500$) and late ($\tau = 50\,000$) stages show that, although the structures undergo considerable coarsening, their basic category of morphology does not change. Hence, the 2D bicontinuous morphology persists throughout time (remaining self-similar), as does the discrete nonwetting morphology. However, the aspect ratio of the height-to-width of the nonwetting domains does change. For the 2DBi morphology, the early structure has tubes of the nonwetting phase that have cross sections that are fairly circular. At latter times, as the widths of the tubes increases, this aspect ratio changes, and the nonwetting domains have a more "flattened" appearance (which is not due to any change in their height, solely the change in their width). The same is true for the discrete domains in Figs. 6(c) and 6(d). This flattening is due to the restriction created by the two wetting layers on the top and bottom of the film.

To provide a more quantitative analysis of the morphology change throughout time, with varying film thickness and film composition, we have calculated the continuity factor (Γ_C) of the nonwetting phase. Figure 7 shows an array of plots of Γ_C versus time, averaged over 20 independent simulations for each condition. The top-to-bottom rows correspond to film thicknesses of $n_z = 26\,\delta$, $20\,\delta$, and $14\,\delta$. The left-to-right columns correspond to film compositions of $\bar{\phi}_{\mathrm{NW}} = 0.25$, 0.2625, 0.275, 0.2875, and 0.3. General trends can be detected: Films with larger thickness and lower $\bar{\phi}_{\mathrm{NW}}$ have discrete (or, discontinuous) nonwetting domains. On the other hand, films with smaller thickness and larger $\bar{\phi}_{\mathrm{NW}}$ have continuous nonwetting domains. Figure 7 illustrates the abrupt transition in morphology as you move left to right and top to bottom with the array of plots. For intermediate values of composition and film thickness, there are morphologies with intermediate values of Γ_C (i.e., $0.25 < \Gamma_C < 0.75$). These systems have morphologies that typically appear bicontinuous, but their largest nonwetting domain is in the range of 25%–75% of the overall nonwetting phase volume, which is generally below a percolation threshold.

This is made evident by the plot in Fig. 8, showing representative snapshots of the morphologies for the same configuration of film thicknesses (rows) and film compositions (columns) as Fig. 7. In Fig. 8, the nonwetting domains are colored according to their respective size, with yellow indicated the largest size. Again, this is accomplished with the Hoshen-Kopelman algorithm. These snapshots show more clearly the

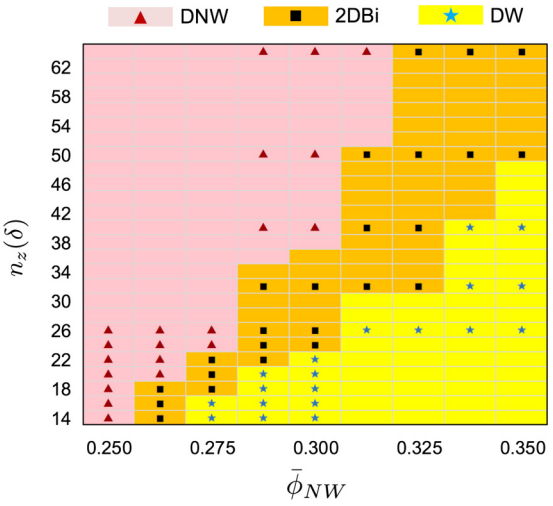

FIG. 9. Morphology map of the multiphase systems with symmetric SDSD with varying composition (x axis) and film thickness (y axis). The discrete and bicontinuous regions are labeled, and the narrow transition region is indicated by the orange band in the middle of the plot, which corresponds with the 2D bicontinuous structure described in the text.

degree of continuity in terms of percolating domains, and the transition in morphology from discrete to bicontinuous for varying composition and film thickness.

Finally, we compiled all of the data from the array of film thicknesses and film compositions and created a morphology map, which is shown in Fig. 9. Figure 9, in fact, also includes additional simulations for thicknesses greater than $n_z = 26\,\delta$ as well as composition values of $\bar{\phi}_{\mathrm{NW}}$ up to 0.350, which was done to greater explore the phase space. The regions of DNW, 2DBi, and DW morphologies are indicated. The 2DBi region exists as a narrow band that separates the DNW and DW regions. For very small thicknesses, below our smallest thickness of $n_z = 14\,\delta$, phase separation is suppressed due to the strong overlapping wetting layers adjacent to the surfaces. As film thickness is increased, the regions for all three morphologies shift right, to greater values of $\bar{\phi}_{\mathrm{NW}}$. The largest film thickness we studied was $n_z = 64$, where both the DNW and the 2DBi morphologies were observed (the DW phase will also form at this thickness when $\bar{\phi}_{\mathrm{NW}} > 0.350$, which we know from previous simulations [34]). Figures 10 and 11 contain images of the morphologies for the larger thicknesses.

The question becomes the following: Will the 2DBi morphology emerge for larger film thicknesses? Or, is there an upper limit for the film thickness where 2DBi morphology can form? The geometrical size of 3D simulations are limited by computing power, so there is a limit to which we can probe this question computationally. Nonetheless, we argue that as long as two parallel surfaces with symmetric wetting conditions are present, all three morphologies may emerge, depending on the composition. We base this conjecture on the fact that in power-law growth regimes, the morphology coarsens in a self-similar manner. In a film with symmetric SDSD, the coarsening structure eventually becomes constricted by the two wetting layers, and a transition to the thin-film morphologies described herein takes place. The time it takes to reach this transition increases with the thickness of the film. Once this transition has taken place, the morphology may have discrete domains of nonwetting phase, or discrete domains of wetting phase, and there should be an intermediate zone with the 2DBi morphology. Observance of the 2DBi morphology at large film thicknesses (i.e., $n_z \gg 64\,\delta$) will require much longer simulation times and much larger simulation domains, and we therefore leave that for future work.

We furthermore point out that our CHC model does not include hydrodynamic effects. The influence of hydrodynamic effects will likely be minimal with the respect to the emergent morphologies observed here, due to the near proximity of the boundaries which will keep Reynolds numbers very low. However, while we do not expect a qualitative influence on morphology, it is known that hydrodynamic flow accelerates the coarsening process, even in SDSD, as examined by Tanaka [19].

IV. CONCLUSIONS

We have investigated how symmetric SDSD is influenced by both the film thickness and film composition using three-dimensional computer simulations. A 2D bicontinuous morphology can develop for certain compositions depending on the film thickness. This 2D bicontinuous morphology persists in time into the late-stage coarsening regime, and remains self-similar after significant coarsening. A morphology map was constructed to illustrate the regions of DNW, 2DBi, and DW morphologies on the film thickness and composition space.

The 2D bicontinuous morphology described here potentially has interesting applications for membrane science. The structure, for example, might be fabricated from a thin film consisting of a binary polymer melt. Following solidification,

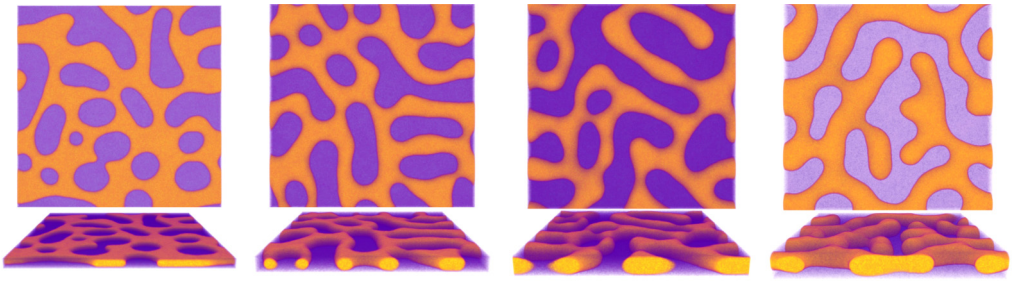

FIG. 10. Thin-film morphologies for a film composition of $\bar{\phi}_{\mathrm{NW}} = 0.35$ with film thickness of (left to right) $n_z = 26$, 40, 50, and 64 δ. The purple shading represents wetting phase and the orange shading represents nonwetting phase. Each image was taken at a simulation time of $\tau = 50\,000$. The two left images were classified as DW morphologies, and the two right images were classified as 2DBi morphologies.

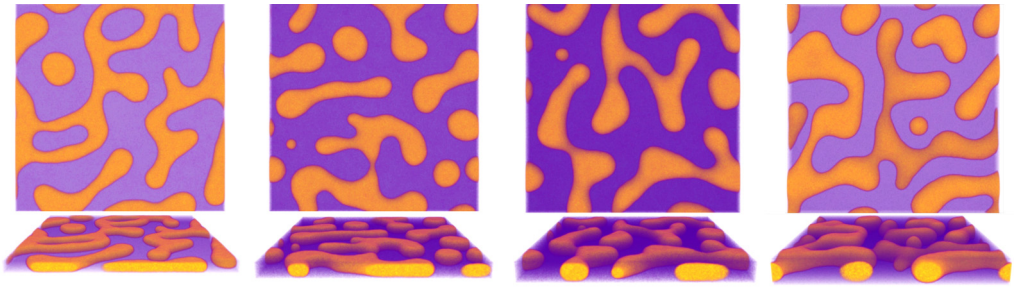

FIG. 11. Same as Fig. 10, but with $\bar{\phi}_{NW} = 0.30$, and film thickness of (left to right) $n_z = 32$, 40, 50, and 64 δ. The leftmost image was classified as 2DBi morphology, and the three right images were classified as DNW morphologies.

either the wetting or the nonwetting phase could be chemically etched. If the wetting phase is etched, a 2D meshlike membrane would remain. On the other hand, if the nonwetting phase were etched, a membrane with internal porosity not accessible from the top or bottom surfaces could be formed. Due to the continuity of the internal porosity, such pore channels could be used to laterally transport medium, for example, with applications such as artificial skin or artificial plant leafs.

ACKNOWLEDGMENTS

The authors acknowledge support from the National Science Foundation under Grant No. 1457888. This research is also supported by the Arkansas High Performance Computing Center, which is funded through multiple National Science Foundation grants and the Arkansas Economic Development Commission.

[1] J. W. Cahn, Phase separation by spinodal decomposition in isotropic systems, J. Chem. Phys. **42**, 93 (1965).
[2] K. Binder and D. Stauffer, Theory for the Slowing Down of the Relaxation and Spinodal Decomposition of Binary Mixtures, Phys. Rev. Lett. **33**, 1006 (1974).
[3] J. S. Huang, W. I. Goldburg, and A. W. Bjerkaas, Study of Phase Separation in a Critical Binary Liquid Mixture: Spinodal Decomposition, Phys. Rev. Lett. **32**, 921 (1974).
[4] S. Nojima, K. Tsutsumi, and T. Nose, Phase separation process in polymer systems. i. light scattering studies on a polystyrene and poly(methylphenylsiloxane) mixture, Polymer Journal **14**, 225 (1982).
[5] K. Binder, Collective diffusion, nucleation, and spinodal decomposition in polymer mixtures, J. Chem. Phys. **79**, 6387 (1983).
[6] S.-W. Song and J. M. Torkelson, Coarsening effects on microstructure formation in isopycnic polymer solutions and membranes produced via thermally induced phase separation, Macromolecules **27**, 6389 (1994).
[7] R. M. Dorin, H. Sai, and U. Wiesner, Hierarchically porous materials from block copolymers, Chem. Mater. **26**, 339 (2013).
[8] L. Li, X. Shen, S. W. Hong, R. C. Hayward, and T. P. Russell, Fabrication of co-continuous nanostructured and porous polymer membranes: Spinodal decomposition of homopolymer and random copolymer blends, Angew. Chem., Int. Ed. **51**, 4089 (2012).
[9] P. Adelhelm, Y.-S. Hu, L. Chuenchom, M. Antonietti, B. Smarsly, and J. Maier, Generation of hierarchical meso- and macroporous carbon from mesophase pitch by spinodal decomposition using polymer templates, Adv. Mater. **19**, 4012 (2007).
[10] E. D. Siggia, Late stages of spinodal decomposition in binary mixtures, Phys. Rev. A **20**, 595 (1979).
[11] P. Guenoun, D. Beysens, and M. Robert, Dynamics of Wetting and Phase Separation, Phys. Rev. Lett. **65**, 2406 (1990).
[12] R. A. L. Jones, L. J. Norton, E. J. Kramer, F. S. Bates, and P. Wiltzius, Surface-Directed Spinodal Decomposition, Phys. Rev. Lett. **66**, 3087 (1991).
[13] P. Wiltzius and A. Cumming, Domain Growth and Wetting in Polymer Mixtures, Phys. Rev. Lett. **66**, 3000 (1991).
[14] F. Bruder and R. Brenn, Spinodal Decomposition in Thin Films of a Polymer Blend, Phys. Rev. Lett. **69**, 624 (1992).
[15] H. Tanaka, Wetting Dynamics in a Confined Symmetric Binary Mixture Undergoing Phase Separation, Phys. Rev. Lett. **70**, 2770 (1993).
[16] M. Geoghegan, R. A. L. Jones, and A. S. Clough, Surface directed spinodal decomposition in a partially miscible polymer blend, J. Chem. Phys. **103**, 2719 (1995).
[17] L. Sung, A. Karim, J. F. Douglas, and C. C. Han, Dimensional Crossover in the Phase Separation Kinetics of Thin Polymer Blend Films, Phys. Rev. Lett. **76**, 4368 (1996).
[18] H. Wang and R. J. Composto, Thin film polymer blends undergoing phase separation and wetting: Identification of early, intermediate, and late stages, J. Chem. Phys. **113**, 10386 (2000).
[19] H. Tanaka, Interplay between wetting and phase separation in binary fluid mixtures: roles of hydrodynamics, J. Phys.: Condens. Matter **13**, 4637 (2001).
[20] K. Binder and H. L. Frisch, Dynamics of surface enrichment: A theory based on the Kawasaki spin-exchange model in the presence of a wall, Z. Phys. B: Condens. Matter **84**, 403 (1991).
[21] S. Puri and K. Binder, Surface-directed spinodal decomposition: Phenomenology and numerical results, Phys. Rev. A **46**, R4487 (1992).
[22] S. Puri and K. Binder, Surface effects on kinetics of ordering, Z. Phys. B: Condens. Matter **86**, 263 (1992).
[23] H. W. Diehl and H. K. Janssen, Boundary conditions for the field theory of dynamic critical behavior in semi-infinite systems with conserved order parameter, Phys. Rev. A **45**, 7145 (1992).
[24] H. Chen and A. Chakrabarti, Surface-directed spinodal decomposition: Hydrodynamic effects, Phys. Rev. E **55**, 5680 (1997).
[25] K. Binder, S. Puri, and H. L. Frisch, Surface-directed spinodal decomposition versus wetting phenomena: Computer simulations, Faraday Discuss. **112**, 103 (1999).

[26] S. Bastea, S. Puri, and J. L. Lebowitz, Surface-directed spinodal decomposition in binary fluid mixtures, Phys. Rev. E **63**, 041513 (2001).

[27] S. Puri and H. L. Frisch, Surface-directed spinodal decomposition: modeling and numerical simulations, J. Phys.: Condens. Matter **9**, 2109 (1997).

[28] S. Puri, Surface-directed spinodal decomposition, J. Phys.: Condens. Matter **17**, R101 (2005).

[29] S. K. Das, S. Puri, J. Horbach, and K. Binder, Kinetics of phase separation in thin films: Simulations for the diffusive case, Phys. Rev. E **72**, 061603 (2005).

[30] S. K. Das, S. Puri, J. Horbach, and K. Binder, Molecular Dynamics Study of Phase Separation Kinetics in Thin Films, Phys. Rev. Lett. **96**, 016107 (2006).

[31] S. Puri, Interplay of wetting and phase separation at surfaces, Phys. A: Stat. Mech. Appl. **384**, 100 (2007).

[32] M. J. A. Hore and M. Laradji, Dissipative particle dynamics simulation of the interplay between spinodal decomposition and wetting in thin film binary fluids, J. Chem. Phys. **132**, 024908 (2010).

[33] H.-J. Chung and R. J. Composto, Breakdown of Dynamic Scaling in Thin Film Binary Liquids Undergoing Phase Separation, Phys. Rev. Lett. **92**, 185704 (2004).

[34] J. M. Carmack and P. C. Millett, Diverse morphologies in thin-film bijels by varying film thickness and composition, Soft Matter **13**, 4214 (2017).

[35] J. Zhu, L.-Q. Chen, J. Shen, and V. Tikare, Coarsening kinetics from a variable-mobility Cahn-Hilliard equation: Application of a semi-implicit fourier spectral method, Phys. Rev. E **60**, 3564 (1999).

[36] S. Frijters, T. Krüger, and J. Harting, Parallelised Hoshen-Kopelman algorithm for lattice-Boltzmann simulations, Comput. Phys. Commun. **189**, 92 (2015).

[37] S. Chaput, C. Carrot, M. Castro, and F. Prochazka, Co-continuity interval in immiscible polymer blends by dynamic mechanical spectroscopy in the molten and solid state, Rheol. Acta **43**, 417 (2004).